UC Berkeley

UC Berkeley Previously Published Works

Title

Synaptic Mechanisms of Feature Coding in the Visual Cortex of Awake Mice

Permalink

https://escholarship.org/uc/item/6xh7z4s3

Journal

Neuron, 95(5)

ISSN

0896-6273

Author

Adesnik, Hillel

Publication Date

2017-08-01

DOI

10.1016/j.neuron.2017.08.014

Peer reviewed

eScholarship.org Powered by the California Digital Library
University of California

Author Manuscript

Author Manuscript

Author Manuscript

Author Manuscript

HHS Public Access

Author manuscript

Neuron. Author manuscript; available in PMC 2018 August 30.

Published in final edited form as:

Neuron. 2017 August 30; 95(5): 1147–1159.e4. doi:10.1016/j.neuron.2017.08.014.

Synaptic mechanisms of feature coding in the visual cortex of awake mice

Hillel Adesnik[1,2,3]

[1]Department of Molecular and Cell Biology, University of California, Berkeley, Berkeley, CA 94720 USA

[2]Helen Wills Neuroscience Institute, University of California, Berkeley, Berkeley, CA 94720 USA

Summary

The synaptic mechanisms of feature coding in the visual cortex are poorly understood, particularly in awake animals. The ratio between excitation (*E*) and inhibition (*I*) might be constant across stimulus space, controlling only the gain and timing of neuronal responses, or it might change, directly contributing to feature coding. Whole-cell recordings in L2/3 of awake mice revealed that the E/I ratio systematically declines with increasing stimulus contrast or size. Suppressing somatostatin neurons enhanced the *E* and *I* underlying size tuning, explaining SOM neurons' role in surround suppression. These data imply that contrast and size tuning result from a combination of a changing E/I ratio and the tuning of total synaptic input. Furthermore, they provide experimental support in awake animals for the 'Stabilized Supralinear Network', a model that explains diverse cortical phenomena, and suggest that a decreasing E/I ratio with increasing cortical drive could contribute to many different cortical computations.

Keywords

Primary visual cortex; V1: E/I balance; size tuning; normalization; contextual modulation; optogenetics; in vivo whole cell; contrast sensitivity; neural coding

Introduction

Neurons are computational devices that transform patterns of synaptic input into sequences of action potential output. In the sensory cortex, intracellular recordings have revealed precise patterns of excitation and inhibition in response to different types of visual stimuli (Anderson et al., 2000; Anderson et al., 2001; Borg-Graham et al., 1998; Contreras and

[3]Lead contact, hadesnik@berkeley.edu.

Publisher's Disclaimer: This is a PDF file of an unedited manuscript that has been accepted for publication. As a service to our customers we are providing this early version of the manuscript. The manuscript will undergo copyediting, typesetting, and review of the resulting proof before it is published in its final citable form. Please note that during the production process errors may be discovered which could affect the content, and all legal disclaimers that apply to the journal pertain.

Author contributions

H.A. conceived of the study, performed the experiments, and wrote the manuscript.

Data and software availability

Raw data and statistical analysis software can be provided on request. Contact hadesnik@berkeley.edu.

Author Manuscript Author Manuscript Author Manuscript Author Manuscript

Palmer, 2003; Douglas et al., 1991; Ferster, 1986; Ferster and Jagadeesh, 1992; Haider et al., 2010; Hirsch et al., 1998; Li et al., 2015; Liu et al., 2010; Priebe and Ferster, 2005). In many cases, excitation (*E*) and inhibition (*I*) maintain a nearly constant ratio across space and time, and this balance is thought to be critical for many aspects of information processing in the cortex (Haider et al., 2006; Higley and Contreras, 2006) (Marino et al., 2005; Okun and Lampl, 2008; Shu et al., 2003; Sun et al., 2010; Wehr and Zador, 2003). In a few other cases, the ratio of *E* and *I* can change, suggesting that a dynamic E/I ratio contributes to feature tuning, sharpening, for example, the tuning to specific orientations of gratings (Li et al., 2012b) or to sound frequency in the auditory cortex (Kato et al., 2017; Wu et al., 2008). However, nearly all these studies, except a few (Bennett et al., 2013; Kato et al., 2017; Perrenoud et al., 2016), have been performed in anesthetized animals, and anesthesia is known to profoundly influence cortical dynamics and synaptic excitation and inhibition (Adesnik et al., 2012; de Kock and Sakmann, 2009; Durand et al., 2016; Ferezou et al., 2006; Greenberg et al., 2014; Haider et al., 2013; Niell and Stryker, 2010; Vaiceliunaite et al., 2013). One recent study in the visual cortex (V1) of awake mice revealed that for one set of stimuli - large vertical bars - inhibitory currents dominate excitatory currents in both time and space (Haider et al., 2013). This result raises the more general question of how *E* and *I* vary across visual stimulus space in wakefulness and during visual processing.

A key question is whether *E* and *I* maintain a constant proportionality as stimulus features are changed, or whether their ratio varies. If the E/I ratio is fixed across stimulus space, tuning to specific features – such as the size or contrast of gratings – would be determined by the tuning of the absolute magnitudes of excitatory and inhibitory inputs, and not any change in their relative strengths. If, instead, the E/I ratio changes it could contribute to feature selectivity itself. Furthermore, the E/I ratio for the same set of stimuli may be different between anesthetized and awake mice, or even might vary between specific behavioral states. Both wakefulness and alertness can preferentially recruit subtypes of inhibitory neurons in V1, such as SOM and VIP cells (Adesnik et al., 2012; Fu et al., 2014; Paken et al., 2016), which could profoundly influence how the E/I ratio changes for different types of stimuli.

Recently, a theoretical model has been put forward to account for a wide array of V1 computations, including surround modulation (e.g., size tuning) and normalization (e.g., contrast saturation), two canonical forms of cortical computation. This model – termed the Stabilized Supralinear Network (SSN) – rests on a few simple assumptions about cortical dynamics, such as the supralinear input/output relationships of single neurons, strong recurrent excitation, and feedback inhibition (Rubin et al., 2015). A key feature of the model is that at low stimulus strengths, the V1 network is dominated by external input, recurrent input is weak, and neurons summate inputs in a supralinear fashion. However, as stimulus strength grows (e.g., in contrast or size) intracortical excitatory recurrence begins to dominate over external input. To prevent saturation, the system moves into an inhibition stabilized network (ISN) regime where summation is much more linear or even sub-linear. This model has garnered experimental support from anesthetized cats (Ozeki et al., 2009; Rubin et al., 2015), but none from awake animals. A central prediction of this model is that the E/I ratio should decline with increasing stimulus strength.

Author Manuscript Author Manuscript Author Manuscript Author Manuscript

To determine if the E/I ratio is constant or dynamic across stimulus space, and in so doing also test core predictions of the SSN model for the first time in awake animals, this study used low-resistance whole cell recordings in V1 of awake mice (Margrie et al., 2002) to measure how single neurons encode visual stimulus features through synaptic *E* and *I*. This study focused particularly on the encoding of visual stimulus contrast and size (Anderson et al., 2000; Anderson et al., 2001; Hubel and Wiesel, 1965), two fundamental stimulus parameters that strongly influence the spiking response of V1 cortical neurons. For increasing contrast, V1 cortical neurons typically show saturation of their spike rates, while for increasing size, they often exhibit suppression when the stimulus extends beyond the classical receptive field (Anderson et al., 2001; Bair et al., 2003; Carandini et al., 1997; Rubin et al., 2015). The synaptic mechanisms that underlie these response properties in the awake brain remain uncertain. Saturation to increasing contrast could be explained purely by *E* and *I* that maintain a constant ratio, but whose absolute magnitudes saturate. Alternatively, a decrementing E/I ratio with increasing contrast could critically contribute to saturation. Similarly, size tuning (a.k.a., surround suppression) could be explained by a suppression of *E* and *I* at larger sizes with no change in their ratio, by a decrease in the E/I balance, or by a mixture of both schemes. The SSN model predicts a mixture: as V1 is driven more strongly, such as with higher contrasts or larger stimulus sizes, the E/I ratio should decrease (Rubin et al., 2015), and when V1 is in the ISN regime the absolute magnitudes of *E* and *I* should also show suppression (Ozeki et al., 2009). Prior studies on these topics performed their experiments in animals under anesthesia (Anderson et al., 2000; Bringuier et al., 1999; Li et al., 2012a; Ozeki et al., 2009). This has left it uncertain how *E* and *I* relate to each other in the awake brain, and whether the SSN model accurately predicts synaptic dynamics during wakefulness.

The data from this study indicate that in awake mice, the E/I ratio is not constant, but instead systematically changes, tilting towards *I* as stimulus contrast or size is increased. The observed *E* and *I* are sufficient to account for contrast saturation of spiking in V1 (Carandini et al., 1997; Maffei and Fiorentini, 1973), and stimulus-size-dependent surround suppression, when tested using dynamic clamp. These data are consistent with the predictions of the SSN model, suggesting that it also captures V1 dynamics of awake mice. The SSN model, as well as previous theoretical work (Ozeki et al., 2009; Tsodyks et al., 1997), predicts that suppression of inhibitory neurons would paradoxically increase inhibitory synaptic input to cortical neurons when the network is in the ISN regime. In agreement with this prediction, optogenetic suppression of SOM neurons, whose activity is critical for surround suppression (Adesnik et al., 2012; Nienborg et al., 2013), profoundly enhanced synaptic inhibition, as well as excitation, as stimulus size was increased, without changing the E/I ratio. This suggests that SOM cells contribute to surround suppression by restricting overall network activity for larger stimuli, but do not control the E/I ratio *per se*. Taken together, these data demonstrate that the E/I ratio varies with elementary stimulus features to help support the encoding of size and contrast in the primary visual cortex. Since the core circuitry supporting the SSN model is likely to be conserved across cortical areas, this suggests that this model, and particularly the declining E/I ratio it predicts for increasing cortical drive, may help account for diverse features of cortical computation.

Author Manuscript Author Manuscript Author Manuscript Author Manuscript

Results

The E/I ratio declines with increasing contrast

Contrast is one of the most basic parameters that characterize stimulus strength in visual cortical neurons. Most mouse V1 neurons show monotonic increases in firing as contrast increases, and then typically begin to saturate below maximum contrast, although a smaller number exhibit band pass or low pass tuning to contrast (Durand et al., 2016). How do *E, I* and the E/I ratio potentially account for the suprathreshold encoding of stimulus contrast? Intracellular whole cell recordings were made in awake mice from a sample of 26 neurons (11 in I_{clamp} and 15 in V_{clamp}) for six levels of contrast, while keeping size and orientation fixed at their preferred values for each cell (Fig. 1A). Consistent with measurements of contrast sensitivity in extracellular recordings in awake mice (Busse et al., 2011; Durand et al., 2016), intracellular current clamp recordings revealed that 8/11 neurons exhibited monotonically increasing relationships between contrast and spiking. A similar analysis on the subthreshold membrane potential changes revealed a parallel result (10/11 neurons). Population curves showed the well-characterized sub-linear relationship between stimulus contrast and spiking and membrane depolarization (Fig. 1B,C). Most sampled neurons fired at the highest rate and showed the strongest mean depolarization for the highest or second to highest presented contrast (see histograms, Fig. 1D), with an estimated 50% of maximum (EC_{50}) of spiking of 56.0±0.1% and for V_m of 42.5±0.1% contrast. The hypothesis that V1 operates as an SSN depends on the idea that the *in vivo* firing rate of neurons as a function of their input is supralinear, i.e. has increasing slope with increasing input (Rubin et al., 2015). Consistent with this notion, plotting the relationship between the time-averaged membrane potential and the instantaneous spike rate across all stimulus conditions revealed a highly supralinear relationship (Figure S2).

Next, to address the underlying synaptic basis for contrast encoding in L2/3 V1 neurons, a series of 15 V_{clamp} recordings were made under similar conditions, but using an internal solution that blocks many voltage gated conductances. By recording at the corresponding reversal potentials for excitation and inhibition, the two opposing conductances can be separately measured. The ability of the somatic voltage to properly separate *E* and *I* is addressed in experiments below.

In principle, *E* and *I* might both increase with contrast, but maintain a constant ratio, or balance. Alternatively, *E* and *I* might grow differentially with contrast, with one more sensitive to contrast than the other. In a third scenario, *I* could conceivably show little variation with contrast, if the high convergence of excitatory axons onto inhibitory cells might drive saturating inhibition at low contrast. Voltage clamp measurements of synaptic *E* and *I* revealed that nearly all neurons exhibited monotonic increases in both *E* and *I* as contrast was increased (see Fig. 2A,B for four examples, and all contrast response functions are shown in Fig. S3). In the mean population response curves, *E* rose at lower contrast levels than *I* (Fig. 3B), and the estimated contrast evoking the half-maximal input (EC_{50}) for *E* (mean: 37±7% contrast) was lower than that of *I* (mean: 50±6% contrast, $p < 0.05$, $n = 13$; sign rank test, Fig. 3C) in the majority of cells with good fits (10/13 cells). Importantly, this resulted in a declining E/I ratio (computed as E/(E+I), see Methods) as a function of

Author Manuscript Author Manuscript Author Manuscript Author Manuscript

stimulus contrast ($p < 0.05$, Kruskal Wallis test), with a mean ratio of 0.51±0.09 at 6–10% contrast, and 0.35±0.05 at 100% contrast, $p < 0.05$ sign rank test, $n = 12$, Fig. 3D). While across the population of recorded cells E and I peaked consistently at higher contrast levels, the E/I ratio tended to peak at lower contrast levels (see histograms, Fig. 3E). These data demonstrate that spiking, membrane potential and synaptic E and I all monotonically increase as stimulus contrast increases, but that the ratio between E and I does not remain fixed, and instead significantly declines at higher contrast. This suggests that the saturation of spiking responses to increasing contrasts could, at least in part, be explained by a declining E/I ratio. Despite this decline, neurons are only rarely tuned to lower contrasts (Durand et al., 2016). This may be explained by the fact that the absolute magnitudes of E and I continue to increase up to the highest contrast.

The E/I ratio declines with increasing stimulus size

Is the declining E/I ratio also true for increasing stimulus size in the awake cortex? To address this question, the influence of stimulus size on the responses of L2/3 V1 neurons was addressed next. It should be noted that size tuning (or surround suppression) is weak in L2/3 in anesthetized mice, but a prominent feature of recordings in awake mice (Adesnik et al., 2012; Nienborg et al., 2013; Vaiceliunaite et al., 2013). These previous findings emphasize that performing these intracellular recordings in the cortex of awake mice is critical. The data set consisted of the responses of 25 L2/3 neurons (5 in I_{clamp} and 20 in V_{clamp}) to six different stimulus sizes (8–55 degrees of visual angle, Fig. 4A). Extracellular recordings have established that the majority of L2/3 neurons in awake mouse V1 (Adesnik et al., 2012; Vaiceliunaite et al., 2013), as in cat and primate V1 (Anderson et al., 2001; Angelucci and Shushruth, 2014; Bair et al., 2003; Blakemore and Tobin, 1972; Gilbert, 1977; Maffei and Fiorentini, 1976; Sceniak et al., 1999), are size tuned, and suppressed by large visual stimuli. Intracellular recordings in awake mice confirmed this finding (Fig. 4B, mean suppression index = 0.65±0.13, 3/5 cells significantly size tuned, $p < 0.05$, Kruskal-Wallis). Subthreshold depolarization was also modestly tuned (mean suppression index of V_m = 0.40±0.16, 3/5 cells significantly tuned, $p < 0.05$, Kruskal-Wallis, Fig. 4C).

Next, voltage clamp measurements of E and I were made to address the underlying synaptic basis of size tuning. Several possible scenarios exist for how E and I might change with size that could underlie size tuning. In a simple scenario, excitation might saturate at small sizes (e.g., the size of the classical receptive field, or CRF), while inhibition might grow with stimuli beyond the CRF, consistent with the known broader spatial tuning of inhibitory neurons (Adesnik et al., 2012). This would result in a declining E/I ratio with stimulus size. Alternatively, both E and I might themselves show size tuning, while their ratio remains constant, supporting the notion that a net reduction in E and I with stimulus size explains surround suppression. In a third scenario, E might be size tuned, but I might grow with size or saturate at intermediate sizes, also resulting in a size-dependent reduction in E/I ratio. Example responses from four different representative neurons are shown in Fig. 5A. As can be seen from these examples, unlike for contrast, L2/3 neurons exhibited varying relationships between E and I as stimulus size was increased (Fig. 5B). Nevertheless, in all these cases, the E/I ratio decreased with increasing stimulus size (Fig. 5C). The tuning of E and I for all 20 recorded neurons is shown in Figure S4, demonstrating the diversity of E and

Author Manuscript Author Manuscript Author Manuscript Author Manuscript

I across cells. Despite this diversity, in most cells both *E* and *I* were significantly tuned (*E*: 15/20 cells, $p<0.05$, Kruskal Wallis, significant effect of stimulus size on synaptic charge, suppression index: 0.29±0.06; *I*: 16/20 cells, $p<0.05$, Kruskal Wallis, suppression index: 0.29±0.05; n = 20), with the population tuning curves for *E* and *I* showing net suppression at larger sizes (Fig. 6A,B). The E/I ratio was lower in 13/20 cells at the largest size than at the smallest size ($p < 0.05$, sign rank test) and the ratio in these cells decreased with size ($p < 0.05$, Kruskal-Wallis, Fig. 6C). 9/20 cells exhibited the highest E/I ratio at the smallest size (Fig. 6D), with the E/I ratio decreasing from 0.48±0.05 to 0.21±0.04 across the six presented stimuli. These data indicate that for visual stimuli of different sizes, the E/I ratio decreases with size, consistent with the SSN model, and the absolute magnitude of and E and I are also often size tuned, a feature consistent with the ISN regime (Ozeki et al., 2009). This suggests that both a changing E/I ratio and suppression of *E* and *I, per se*, combine to lead to the potent size tuning of L2/3 V1 cortical neurons.

The somatic voltage clamp separates excitatory and inhibitory synaptic currents

An important concern for any study relying on the somatic voltage clamp to separate *E* and *I* is the ability to clamp synapses at their corresponding reversal potentials. Previous theoretical work, and empirical measurements in rat layer 5 (L5) pyramidal cells, indicate that somatic voltage clamp may only poorly control dendritic or synaptic voltage (Bar-Yehuda and Korngreen, 2008; Chadderton et al., 2014; Hausser and Roth, 1997; Poleg-Polsky and Diamond, 2011; Williams and Mitchell, 2008). However, mouse L2/3 pyramidal cells are much more compact than rat L5 pyramidal cells, and for the experiments in this study multiple, broad spectrum blockers of intrinsic conductances were used to optimize space clamp. To address empirically how well the somatic voltage clamp controls synaptic voltage in L2/3 pyramidal cells under the conditions used here, ‘sCRACM’ (sub-cellular ChR2-assisted circuit mapping) (Petreanu et al., 2009) was used to optogenetically activate synapses at defined distances from the soma in brain slices. In this approach, measuring how the reversal potential of *E* or *I* varies with synapse distance from the soma should provide a quantitative estimate of local synaptic voltage control by the somatic electrode. If synaptic voltage does approach the command voltage, the reversal potential of any synaptic conductance (GABA, NMDA, or AMPA) should vary only slightly with distance. If, on the other hand, the somatic pipette only poorly controls synaptic voltage, the reversal potential of distant synaptic currents will diverge substantially from its expected value.

To this end, ChR2 was expressed in cortical neurons (using emx1-Cre, SOM-Cre, or wild type mice, see Methods), and synapses at specific distances were photo-stimulated using a digital micro-mirror device (Fig. 7A). The full-width half maximum (FWHM) of the optical system along the vertical axis was estimated to be 19±2 μm by measuring ChR2 photocurrents in cultured Chinese Hamster Ovary cells (Fig. 7B). Accordingly, a bar of light was projected onto the neuron and moved in 25 μm increments along the vertical axis of the cortex (typically aligned with the main apical dendrite) to stimulate sets of synapses at progressively more distant locations from the somatic voltage clamp pipette. Example traces of light evoked GABA, NMDA, and AMPA currents at different somatic command potentials and increasing distance are presented in Fig. 7C. Consistent with their more distal location, for example, the estimated 10–90% rise time of evoked IPSCs increased

Author Manuscript Author Manuscript Author Manuscript Author Manuscript

significantly with increasing distance (Fig. 7D). The difference in the measured reversal potential of all three conductances increased at progressively more distant synapses ($p < 0.05$, Kruskal-Wallis Anova), but only slightly (Fig. 7E–H). For example, at 150 μm, the error in the measured GABA reversal was 4±1 mV; for NMDA it was 3.0±0.5 mV, and for AMPA it was 2.1±0.7 mV. Importantly, since during the *in vivo* experiments *E* and *I* were measured with an approximately 70 mV driving force (see Methods) this deviation of reversal at distant synapses should only slightly affect the separation of *E* and *I*. Furthermore, since many, if not most of the synapses onto L2/3 pyramidal neurons are within this distance from the soma, these data indicate that under these conditions the synaptic voltage can be controlled well enough to separate *E* and *I* with the voltage clamp approach with only a minor error.

Excitatory and inhibitory input are sufficient to account for visual stimulus tuning

If the observed changes in *E* and *I* are sufficient to reproduce the non-linear responses of L2/3 V1 neurons to stimuli of increasing contrast or size, then injecting them into a model L2/3 neuron should recapitulate contrast saturation and size tuning. To test this notion, the *E* and *I* conductance traces that were measured using somatic voltage clamp *in vivo* were injected via a dynamic clamp into L2/3 pyramidal neurons in acute V1 cortical slices. Background synaptic input was simulated by injecting noisy, constant barrages of *E* and *I* (see Methods), mimicking what was observed in the absence of any visual stimulus (Chance et al., 2002). Consistent with the notion that the observed *E* and *I* conductances, on their own, are sufficient to generate contrast saturation and size tuning, the dynamically clamped neurons exhibited both properties when injected with the measured *E* and *I* responses (Fig. S5). These data do not exclude important contributions from other conductances in the generation of saturation of size tuning, such as voltage dependent channels in the dendrites (Smith et al., 2013) that may sharpen size tuning or modify saturation. Yet they argue that the stimulus dependence of *E, I* and their ratio that was observed *in vivo* are sufficient to account for an important component of contrast saturation and size tuning.

SOM neurons contribute to size tuning by suppressing both *E* and *I*

What inhibitory circuits might play a role in the non-linear response functions of V1 neurons? For size tuning, previous data has pointed to a crucial role of SOM inhibitory neurons, as optogenetic manipulation of SOM interneurons alters the size tuning of L2/3 visual cortical neurons (Adesnik et al., 2012; Nienborg et al., 2013). SOM neurons, which are very weakly active under anesthesia, but highly active in awake conditions for specific visual stimuli (Adesnik et al., 2012), could control the E/I ratio that contributes to size tuning in awake animals. Since SOM neurons increase their firing rates as stimulus size increases, they could directly contribute to the decrementing E/I ratio observed with larger stimuli through monosynaptic inhibition of pyramidal cells. Alternatively, they might not alter the size tuning of the E/I ratio *per se*, but simply help drive the size-dependent suppression of *E* and *I* input as stimulus size increases. To distinguish between these two possibilities, a set of intracellular voltage clamp recordings from L2/3 neurons were made in awake SOM-Cre mice injected with Cre-dependent AAV driving expression of the optogenetic silencer, eNphR3.0 (Gradinaru et al., 2010). Control trials were interleaved with trials in which the cortex was illuminated with an optic fiber coupled to a red LED. Under

Author Manuscript Author Manuscript Author Manuscript Author Manuscript

identical experimental conditions, extracellular recording from SOM cells revealed a 67±8% decrease in SOM firing for the largest stimulus size (Veit et al., 2017). Consistent with the reduced surround suppression observed during their inactivation (~30% decrease for ~57% suppression of SOM firing) (Adesnik et al., 2012), optogenetic suppression of SOM cells substantially *increased* both visually evoked *E* and *I* (E: $p < 0.0005$, I: $p < 0.005$, two-way-ANOVA, n = 8, Figure 8B,C), but did not eliminate the size-dependent decrement in the E/I ratio ($p > 0.05$, two-way-ANOVA, Fig. 8D). Control experiments with identical illumination of mice not expressing eNpHR3.0 showed no effect of light, ruling out any influence of the optogenetic light itself in modulating normal visual responses ($p > 0.05$, n = 6 cells, two-way-ANOVA, Fig. S6). Additionally, although in SOMCre mice a small number of PV neurons express Cre (3.6%, Fig. S7A,D)(Hu et al., 2013), under the conditions used here no expression of eNpHR3.0 was detected in SOM-Cre^+;PV^+ neurons (0/23 Cre^+/PV^+ cells, Fig. S7A–D).

Therefore, these data provide critical optogenetic confirmation of a core prediction of the SSN when in the ISN regime (Ozeki et al., 2009; Tsodyks et al., 1997), namely, that suppression of inhibitory cells should paradoxically increase inhibitory currents (Litwin-Kumar et al., 2016). These data demonstrate that the normal activity of SOM neurons is critical for regulating the *E* and *I* that underlie size tuning – controlling their absolute magnitude but not how their balance decrements with size – in order to help enforce size tuning, which may be a particular feature of the cortex in awake or alert states.

Discussion

Using whole cell recordings in awake mice the data presented here provide a direct view into the underlying mechanisms for the encoding of two key elementary features of visual stimuli, namely, contrast and size. Furthermore, they provide critical validation to core predictions of the SSN model in awake animals, and also help establish that the visual cortex of awake animals can operate as an ISN. The first principal to emerge from these data is that for increasing contrast or increasing size, the E/I ratio is not fixed, but declines for higher contrast or larger stimuli. With respect to increasing contrast, the data further show that *E* and *I* nearly always monotonically increase towards saturation, in line with that of contrast-evoked spiking and membrane depolarization. Thus, the synaptic measurements provide an explanation for the encoding of contrast by superficial V1 neurons: increasing contrast drives increases in both *E* and *I* that increasingly depolarize the neuron to spike threshold. However, as contrast increases, the E/I ratio systematically declines (Figure 2), and at the same time the absolute magnitudes of *E* and *I* begin to saturate. The combination of saturating *E* and *I* and a declining E/I ratio can then account for the saturation of neuronal firing to contrast.

Similarly, the E/I ratio also decreased with increasing stimulus size, and the absolute magnitudes of *E* and *I* were often highly size-tuned themselves. How does this help distinguish between possible models of size tuning? One model proposes that as stimulus size increases, *I* would increase, driving suppression to larger stimuli (Adesnik et al., 2012), and thus decrease *E* and the E/I ratio. This model is based on the finding that interneurons, particularly those of the SOM subtype, fire much more robustly to larger stimulus sizes than

Author Manuscript Author Manuscript Author Manuscript Author Manuscript

excitatory neurons. An alternative model, with experimental support from anesthetized cats, is that V1, when operating as an ISN, would exhibit strong reductions in both *E* and *I* with increasing size (Ozeki et al., 2009), and this net decrease in overall synaptic conductance (and not necessarily a change in E/I ratio) is what drives surround suppression. The SSN model proposes a hybrid of these ideas: both *E* and *I* should be reduced with increasing size (as predicted by the ISN), because the SSN model operates in the ISN regime, except when driven weakly. However, the SSN also predicts that *E* should decrease more than *I* would, as stimulus size increases, lowering the E/I ratio. Among these three scenarios, the data presented here support the SSN model's predictions. In most recorded cells, *E* was suppressed as stimulus size increased, but the E/I ratio also decreased. Thus, while the suppression of E is surely critical for size tuning (Sato et al., 2016), the decreasing E/I ratio should amplify the net effect of *E* suppression to produce the very strong size tuning of L2/3 cortical neurons. Additional mechanisms for size tuning are also likely to contribute (Bair et al., 2003; Bolz and Gilbert, 1986; Litwin-Kumar et al., 2016; Nurminen and Angelucci, 2014; Ozeki et al., 2004), and taking into account the complexity and sub-cellular localization of inhibitory circuits and other cortical layers and areas is essential for a fuller explanation. One alternative notion that could also explain the declining E/I ratio with contrast and size is for a sub-class of inhibitory neurons (such as SOM neurons) to be less sensitive but have higher gain to visual stimuli than excitatory neurons, a question that could be further addressed with targeted recordings from inhibitory cells in the future. This has been proposed as a key mechanism for the contrast-dependence of surround suppression (Shushruth et al., 2012). Direct recordings of *E* and *I* in awake animals underlying both the contrast and orientation tuning of surround suppression would provide further critical tests of the varying models of surround modulation in V1.

Previously, it was demonstrated that optogenetically suppressing SOM cells impairs size tuning in V1 (Adesnik et al., 2012). How can this result be understood in the context of the data on synaptic *E* and *I* presented here? Figure 8 demonstrates that inactivating SOM cells increases both *E* and *I* in L2/3 cortical neurons. The increase in total synaptic input can explain why SOM suppression disinhibits L2/3 excitatory neurons and reduces size tuning. Simply put, SOM neuron activity suppresses both *E* and *I*, which leads to size tuning; inactivating SOM neurons diminishes the suppression of total synaptic input, impairing normal size tuning. Superficially, the increase in *I* seems paradoxical, as the direct inhibition from SOM cells should be reduced. However, this paradoxical effect is precisely a core prediction of the ISN regime (Litwin-Kumar et al., 2016; Rubin et al., 2015; Tsodyks et al., 1997); when SOM cells are suppressed, PV cells firing rates substantially increase (Veit et al., 2017). In the ISN model, the increased activity of PV cells is a result of increased drive from L2/3 excitatory neurons (which are net disinhibited). The increased activity of PV neurons drives net increases in inhibitory currents in excitatory neurons. A second explanation for the increase in *I* that does not invoke ISN dynamics is that SOM cells directly inhibit PV neurons (Pfeffer et al., 2013), and thus suppressing SOM cells should result in increased somatic inhibition in pyramidal cells since PV neurons are themselves disinhibited (Veit et al., 2017). The data presented here are similar to what has been recently found for sound frequency tuning in the awake auditory cortex (Kato et al., 2017), implying these might be general mechanisms for feature coding across sensory cortex.

Author Manuscript Author Manuscript Author Manuscript Author Manuscript

A second finding is that SOM suppression did not significantly impair the way the E/I ratio declined with stimulus size. This implies that the size tuning of the E/I ratio *per se* is not under direct control of SOM neurons. Instead, SOM cells drive surround suppression by causing a balanced suppression of total synaptic conductance. Optogenetic suppression of SOM cells does not entirely abolish the size tuning of *E, I* or spiking, which is either due to the fact that SOM cells were not completely suppressed here, V1 still operates in the ISN regime in the absence of SOM cells (as is expected), or other mechanisms yet to be clarified. In any case, although both *E* and *I* are suppressed when large stimulus sizes recruit increased SOM cell firing, their balance is preserved. Thus the declining E/I ratio for increasing stimulus size may instead be a consequence of the recurrent dynamics between PV neurons and pyramidal cells.

Taken together, these data provide key insight into the synaptic basis of visual computation in the primary visual cortex of awake animals. Furthermore, they validate core predictions of the SSN model and the ISN regime in awake animals. These include the supralinear input/output relationships of single neurons (Fig. S2), the declining E/I ratio with increasing contrast and size (Fig. 3 and 6), the net suppression of *E* and *I* with stimulus size (Fig. 6), and the paradoxical increase of synaptic inhibition when SOM cells are suppressed (Fig. 8). Future experiments, combining intracellular recordings with simultaneous population imaging and spatially precise optogenetics will be able to further distinguish between competing models of V1 function, and unveil how the diversity and complexity of visual cortical circuits drives vision.

STAR Methods

Lead contact: Hillel Adesnik, hadesnik@berkeley.edu

Contact and Resource Sharing

Further information and requests for resources and reagents should be directed to and will be fulfilled by the Lead Contact, Hillel Aadesni, hadesnik@berkeley.edu.

Experimental model and subject details

All procedures were approved by the University of California, Berkeley ACUC. Wild type (C57;B6 × ICR white), emx1-IRES-Cre, and SOM-IRES-Cre mice were used. Mice of both sexes were used equally, and no differences were observed between sexes. For *in vivo* recordings mice were 5–14 weeks old. For *in vitro* recordings mice were 3–4 weeks old.

Method Details

Animals: surgery and electrophysiological recording—Mice were headplated under isoflurane (1.5–2%) anesthesia with a small stainless steel plate, attached to the skull with Metabond. The skull was protected with cyanoacrylate glue and dental cement (Orthojet). 1–7 days post surgery, Mice were habituated to run freely on a small, 6” diameter rotating disc during head fixation. On the day of surgery mice were anesthetized with 1.5–2% isoflurane and a small craniotomoy was made over V1 by removing the dental cement and slowly thinning the skull until it was transparent with a 0.25 mm carbide burr. A small

Author Manuscript Author Manuscript Author Manuscript Author Manuscript

stainless steel needle (27G) was used to open a hole ~150–500 um in diameter over V1 with no or minimal bleeding. The dura was always left intact. The craniotomy was covered with sterile saline and the animal was allowed to recover under fixation for 15–30 minutes prior to whole-cell recording. Animals typically began running on the treadmill immediately upon arousal, and either continuously or intermittently thereafter. Locomotion speed was measured with a rotary encoder upon which the treadmill was mounted (US Digital, H6), converted to an analog voltage via an Etach2 tachometer (US Digital), and digitized to disk. A threshold of 2.54 cm/s run speed was used to separate running and non-running trials. Under these experimental conditions mouse move their eyes only infrequently, and most ocular deviations are too small to significantly impact neuronal responses (Adesnik et al., 2012), and the pupil was not tracked.

Electrophysiology—Prior to intracellular experiments, a patch pipette filled with ACSF (in mM: NaCl 119, KCl 2.5, $MgSO_4$ 1.3, NaH_2PO_4 1.3, glucose 20, $NaHCO_3$ 26, $CaCl_2$ 2.5) was lowered slowly into the L2/3 under visual guidance (Leica MZ6 stereomicroscope). Using multiunit activity and the LFP as a guide, the visual receptive field of the corresponding location for subsequent whole cell recording was mapped via a hand-controlled small circle (~5 degrees) of changing contrast on the visual stimulus monitor (more details below). This electrode was then removed, and patch pipettes were then inserted in same manner for intracellular recording containing: $CsMeSO_4$ (for voltage clamp) or KGluconate (for current clamp) 135 mM, NaCl 8 mM, HEPES 10 mM, Na_3GTP 0.3 mM, MgATP 4 mM, EGTA 0.3 mM, QX-314-Cl 5 mM (voltage clamp only), TEA-Cl 5mM (voltage clamp only). Although the cells were patched with the blind approach, the conditions used have been reported to strongly bias recording to regular-spiking putative pyramidal cells (Liu et al., 2009). Nevertheless, the data reported here is likely to come from a mix of cell types, dominated nevertheless by excitatory neurons, which make up the majority of L2/3 cells. SOM-Cre mice were injected with AAV viruses (here, AAV9-DIO-EF1a-eNpHR3.0-YFP, UPenn vector core). For optogenetics experiments in SOM-Cre mice all dental cement was premixed with black iron oxide powder to prevent light leakage between the optical fiber for light delivery and the eyes.

Under these conditions, in V_{clamp}, the mean series resistance, prior to any compensation, was 18±1 MΩ across the recording sessions, and fairly stable (Figure S1A,B). It is now well established that locomotion and/or brain state influence spontaneous activity and sensory responses in V1(Ayaz et al., 2013; Niell and Stryker, 2008; Reimer et al., 2014; Vinck et al., 2015), although the exact mechanisms underlying these changes remain a matter of debate (Fu et al., 2014; Paken et al., 2016; Polack et al., 2013). Consistent with prior findings, during locomotion (Bennett et al., 2013), visually evoked *E* and *I* were significantly increased (*E*: not running: 70±6 pC/s, running: 81±8 pC/s, n = 39 cells, $p < 0.005$; *I*: not running: 114±12 pC/s, running: 159±20 pC/s, n = 39 cells, p <0 .005, Wilcoxon sign rank test, Figure S1C,D). Conversely, spontaneous excitation and inhibition, as well as the mean input conductance in the absence of a stimulus showed no significant change (*E*: $p = 0.9$; *I*: $p = 0.4$, input resistance: $p = 0.93$, n = 39 cells, Wilcoxon sign rank test, Figure S1E–G).

Both extracellular and intracellular experiments employed an Axopatch 200B amplifier. All data was acquired with custom software written in Matlab using a National Instruments

Author Manuscript Author Manuscript Author Manuscript Author Manuscript

PCIe-6353 card. Glass pipettes (Sutter instruments) containing either a potassium based internal (for measurements of membrane potential and spiking) or cesium (with added QX-314-Cl, and tetraethylammoniaum-Cl) for voltage clamp recording, were used. Pipettes were pulled on a Sutter P1000 puller in a two stage pull to a long taper pipette of a resistance between 3–5 MOhm. To insert the electrode into the small craniotomy, the ACSF on the skull was removed and the craniotomy briefly dried with compressed air. The electrode was mounted on a Sutter MP285 manipulator, lowered until it nearly reached the brain surface, then the chamber formed by the headplate and cement was re-filled with ACSF, all under visual guidance. The pipette resistance was checked via an oscilloscope and a constant 5 mV voltage step in voltage clamp. High positive pressure (~150 mbar) was applied to the pipette, and it was lowered until a brief and rapid increase in pipette resistance was observed, indicating contact with the dura. The pipette was zeroed to obtain an accurate measurement of recording depth, and then the pipette was advanced quickly through dura, and only pipettes that quickly returned to their baseline resistance were advanced further, otherwise they were exchanged for a fresh pipette and the process was repeated. Once inside the brain the pressure was quickly lowered to 10–30 mBar to search for L2/3 neurons via abrupt, 'bounce' like changes in pipette resistance indicating contact with a plasma membrane, using pulsatile steps of the manipulator (1–2 microns). Upon apparent contact, pipette pressure was released, and slight positive pressure was used to obtain a gigaohm seal. Pipette capacitance was then neutralized and the membrane ruptured by brief suction pulses. Upon rupture the whole cell access was optimized by either slow negative or (more typically) positive pressure and locked off. In the first 2–4 minutes the receptive field of the cell (either via membrane potential, spiking, or excitatory current, command potential = −70 mV) was remapped in the same manner as above, to center the stimulus on the recorded cell's receptive field (almost always aligned with the previous measurement from extracellular recording). The orientation of the stimulus was also optimized for each cell. After spontaneous and evoked responses stabilized (typically 2–4 minutes) experiments were commenced. Membrane potential was obtained in voltage following (current clamp) mode with no current injection. For voltage clamped cells, cells were clamped either at −70 mV to measure synaptic excitation (approximate reversal potential for inhibition), or at +10 mV to measure synaptic inhibition (approximate reversal potential for excitation), uncorrected for the junction potential. Series resistance was monitored on every trial with a negative voltage step. Cells were only included if their series resistance stayed within 20% of their initial value, passively or by adjusting pipette pressure.

Visual stimulation—Visual stimuli were generated with Psychophysics toolbox (Brainard, 1997) using custom software in Matlab (Mathworks) and presented on a gamma corrected 23-inch Eizo FORIS FS2333 LCD display with a 60-Hz refresh rate. Stimuli consisted of drifting square wave gratings with contrast, size, or orientation varied, while all other parameters remained fixed, at 0.04 cycles per degree and 2–2.5 cycles per second. In experiments with varying contrast, size was fixed at 12 degrees, and the orientation fixed at the preferred orientation of the cell (measured via spike rate, V_m depolarization, or mean synaptic excitation). In 7/12 cells contrast was varied in six log increment from 1–100%, and in 5/12 cells from 10–100%. Fig. 3E combines the data from all 12 cells into 6 contrast levels. In experiments with varying size, contrast was set at 100% at the orientation set as

Author Manuscript Author Manuscript Author Manuscript Author Manuscript

above. The grating drifted immediately upon display, and lasted 0.6–1.5 seconds. Inter-trial-intervals (grey screen) lasted from 1.5–3 seconds.

In vivo optogenetics—SOM-Cre were injected neonatally (P3–P5) with AAV9.EF1a.DlO.eNPHR3.0-EYFp.WPRE.hGH prepared by the University of Pennsylvania Vector core. ~20 nL undiluted virus was injected with a Drummond Nanoject into cryoanesthetized neonates at 2–3 locations in V1 (~1.5–2 mm lateral to the labmad suture). During the experiment red light from a Spectra X solid state light source (Lumencor) or a Thorlabs fiber coupled 633 nm LED carried via a 1 mm multimode optic fiber (thorlabs) was used to broadly illuminate all of V1. The fiber was positioned ~2–3 mm from the craniotomy. Illumination trials were interleaved with control trials, and the light was turned on 100 ms after the onset of the visual stimulus, for 450–500 ms. Light intensity was ~4 mW/mm^2. For control experiments, wild type mice (i.e., Cre-negative) were used.

Dynamic Clamp electrophysiology—Brain slices were prepared from 3–4 week old mice of both sexes as previously described (Adesnik et al., 2012). Two independent analog dynamic clamp amplifiers were used, one to compute I_E, the excitatory synaptic current, and the other to compute I_I, the inhibitory synaptic current. The outputs of two the amplifiers were summed with a custom analog summing circuit of equivalent bandwidth. Background synaptic conductance was generated by simulating random barrages of Poisson like inputs with mean rates for *I* = 700 events/second, and *E* = 300 events/second, with rise times of 0.1 ms (both for *E* and *I*), and decay times of 5 ms for *E* and 10 ms for *I*. The amplitudes of the unitary conductances were set to be equal, which, with these parameters, produced an approximately balanced E/I conductance (that is, ~1:1). The visually evoked *E* and *I* were taken from individual cells recorded *in vivo* by averaging individual trials in each cell. The equation implemented by the sum of the two dynamic clamp amplifiers was $I_{syn} = g_E(E_E - V_m) + g_I(E_I - V_m)$. E_E, the reversal potential for excitation, was set to 0 mV, and E_I, the reversal potential for inhibition, was set to 10–20 mV below action potential threshold, typically −60 mV. g_E and g_I were the sum of the visually evoked conductance and the simulated background conductance, for both *E* and *I*. Cells were injected with a constant current through the patch clamp amplifier to depolarize the cell to ~−60–65 mV to facilitate spiking. For the *E* and *I* measured for stimulus contrast, the amplitude of the unitary background conductances was set so that the net spontaneous conductance was subthreshold – in other words, no spontaneous firing was evoked, and all evoked spikes were due to the simulated visually evoked conductances. For the *E* and *I* measured for stimulus size, the amplitude of the unitary background conductances was scaled to drive a spontaneous firing rate of 5–10 Hz. This was necessary because many E/I combinations measured for stimulus size evoked firing at only one or two sizes. For analysis of these experiments the average spontaneous firing rate (computed in a running average across five consecutive trials) was subtracted from the firing rate measured during the injection of the simulated visually evoked conductances, to obtain an evoked rate. The plots in Fig. S5 represent the average across all pairs of E/I combinations measured *in vivo* (from 9 cells for contrast and 12 cells for size), averaged across all dynamically clamped cells (n = 9 for contrast, n = 13 for size).

Author Manuscript Author Manuscript Author Manuscript Author Manuscript

sCRACM-based assessment of the somatic voltage clamp—ChR2 was expressed in cortical neurons using AAV vectors injected neonatally (P2–P5). To evoke IPSCs, ChR2 was expressed selectively in SOM neurons (AAV9.CAGGS.Flex.ChR2-tdTomato.WPRE.SV40, UPenn vector core, into SOM-Cre mice). For evoking EPSCs, ChR2 was expressed selectively in excitatory neurons in emx1-Cre mice, or in all cell types using a cell-type non-selective virus (AAV1-CAG-hChR2(H134R)-mCherry). All viruses were from the UPenn Vector Core. For sCRACM, experiments were performed in the presence of tetrodotoxin (1 μM) and 4-aminopyridine (200–300 μM) to permit direct photo-stimulation of synaptic release in the absence of action potentials. GABA, NMDA or AMPA currents were pharmacologically isolated from each other in separate experiments using appropriate combinations of NBQX (10 μM), R-CPP (10 μM), or picrotoxin (100 μM) (Abcam). When measuring excitation onto pyramidal cells, some of the patched neurons expressed ChR2 themselves. For measuring NMDA currents the synaptic charge was integrated from 0.2–0.3 seconds after the light pulse to ensure the ChR2 photo-current had decayed. For measuring AMPA, cells with appreciable ChR2 current were excluded from analysis by noting a current response that rose with sub-millisecond latency at the onset of the light pulse. A bar of light ~6 × 80 microns in spatial extent, ~20 mW/mm^2, and oriented orthogonal to the main apical dendrite, was projected onto a patched L2/3 neuron using a CEL5500 (Digital Light Innovations) digital micromirror device and a 40× objective (Olympus), and presented at different distances from the soma in a random sequence (0–225 microns, see Figure 7A) by moving the microscope (Sutter SOM scope) through custom software (Matlab). The light source was a 1 Watt 455 nm diode laser (Ultralasers), coupled to the DMD with a liquid light guide. A single L2/3 pyramidal cell was patched with the same internal solution as used *in vivo*, and the holding potential was stepped through a series of voltages to obtain measurements for constructing I–V curves for each conductance. To quantify the spatial resolution of this photo-stimulation protocol, ChR2 was transfected into cultured CHO cells, and circular-shaped cells (~10 μm in diameter) were patched and photo-stimulated in an identical fashion as were neurons. Response functions were fit with a double exponential and the distance providing the estimated half maximal-current was doubled to provide the FWHM of the system. Note that the observed synaptic currents were typically strongest closest to the soma), which is most likely due to a combination of their proximal location and the fact that the closest light bar also activated excitatory and inhibitory synapses on the basal dendrites close to the soma.

Immunohistochemistry—Animals were perfused transcardially with 4% paraformaldehyde, post-fixed for 1–2 days, sunk in sucrose, and sectioned on a freezing microtome. 40 micron sections were incubated in 0.5mL of blocking solution for 1 hour at 4 degrees, then incubated overnight at 4 degrees in blocking solution with 1:1000 dilution of the primary antibody (Rabbit Anti-Parvalbumin, PV 27, Swant). Sections were washed in PBS-T, then incubated in blocking solution containing 1:1000 dilution of secondary antibody (Alexa Fluor 405 Goat Anti-Rabbit A31556, Thermo Fisher Scientific). Z-stack images were taken on an Olympus FV1000 microscope for post-hoc analysis. Stereology was performed manually in ImageJ.

Author Manuscript Author Manuscript Author Manuscript Author Manuscript

Quantification and Statistical Analysis

All quantification and statistical analysis was performed in the Matlab environment. Spikes were automatically detected in current clamp recordings using 0 mV threshold crossing. Membrane potential was measured after filtering traces with a 5 ms median filter to remove spikes. All reported values are from measurements of mean V_m during the visual stimulus. Excitation and inhibition were computed by measuring the charge (i.e., integral of synaptic current using trapezoidal integration); for contrast, the first 1000 ms after visual stimulus onset were integrated; for size, the first 500 ms were integrated, although no difference was seen when analyzing either period in cells presented with longer stimuli. Measurements of spontaneous E and I were made with a grey screen (no contrast in the stimulus). Due to the high background rate of spontaneous excitatory and inhibitory currents, a trial-specific period of the baseline (i.e., between visual stimuli) was first used for subtraction in each trial to provide a baseline for measurements during the visual stimulus. This period was chosen by automatically detecting the 100 ms of lowest variance of membrane potential or membrane current during the immediately preceding inter-stimulus-interval. Following calculation of mean responses for computing tuning functions, tuning curves were further baselined by subtracting the mean synaptic charge measured during the inter-trial interval (grey screen).

All contrast responses functions were fitted with the Naka-Rushton function to obtain estimates of the underlying EC_{50}s. EC_{50} values for two cells in Figure 3 with poor fits were excluded from analysis. The E/I ratio was computed as the mean excitation divided by the sum of the excitation and inhibition, E/(E + I). Population statistics on the E/I ratio were performed following normalizing to the E/I ratio for each cell at the highest contrast or largest size. The suppression index was computed as the response at the maximum stimulus size, divided by the response at the stimulus size that evoked the peak response. Statistical analysis on contrast or size tuning functions was performed with the non-parametric Kruskal-Wallis test after normalization to the peak of each tuning curve. To analyze the relationship between V_m and spike rate (Figure S2), spikes and V_m were analyzed in 300 ms bins across the duration of all current clamp experiments. The resulting relationship between mean V_m and instantaneous spike rate were computed and plotted. Action potential threshold was computed as the membrane potential at action potential onset, defined as the point of maximum positive slope in the phase space of the membrane potential and its first derivative (Sekerli et al., 2004). Sample sizes (cells) and the type of statistical test used for each analysis are indicated in the main text. All tests were non-parametric, except for the two-way ANOVA test. No data was excluded unless the cell quality did not meet the criteria described above. Error bar are always s.e.m.

Supplementary Material

Refer to Web version on PubMed Central for supplementary material.

Acknowledgments

The author is grateful for a critical reading of the manuscript by K. Miller, M. Feller, D. Feldman, and additional discussions with J. Veit and M. Scanziani. The author is grateful for technical support from Desiree Chu, Chris

Author Manuscript Author Manuscript Author Manuscript Author Manuscript

Douglas, David Taylor and Savitha Sridharan. H.A. is a New York Stem Cell Foundation-Robertson Investigator. This work was supported by The New York Stem Cell Foundation and National Eye Institute R01EY023756-01.

References

Adesnik H, Bruns W, Taniguchi H, Huang ZJ, Scanziani M. A neural circuit for spatial summation in visual cortex. Nature. 2012; 490:226–231. [PubMed: 23060193]

Anderson JS, Carandini M, Ferster D. Orientation tuning of input conductance, excitation, and inhibition in cat primary visual cortex. Journal of neurophysiology. 2000; 84:909–926. [PubMed: 10938316]

Anderson JS, Lampl I, Gillespie DC, Ferster D. Membrane potential and conductance changes underlying length tuning of cells in cat primary visual cortex. Journal of Neuroscience. 2001; 21:2104–2112. [PubMed: 11245694]

Angelucci A, Shushruth S. Beyond the Classical Receptive Field: Surround Modulation in Primary Visual Cortex. New Visual Neurosciences. 2014:425–444.

Ayaz A, Saleem AB, Scholvinck ML, Carandini M. Locomotion Controls Spatial Integration in Mouse Visual Cortex. Curr Biol. 2013; 23:890–894. [PubMed: 23664971]

Bair W, Cavanaugh JR, Movshon JA. Time course and time-distance relationships for surround suppression in macaque V1 neurons. Journal of Neuroscience. 2003; 23:7690–7701. [PubMed: 12930809]

Bar-Yehuda D, Korngreen A. Space-clamp problems when voltage clamping neurons expressing voltage-gated conductances. Journal of neurophysiology. 2008; 99:1127–1136. [PubMed: 18184885]

Bennett C, Arroyo S, Hestrin S. Subthreshold Mechanisms Underlying State-Dependent Modulation of Visual Responses. Neuron. 2013; 80:350–357. [PubMed: 24139040]

Blakemore C, Tobin EA. Lateral Inhibition between Orientation Detectors in Cats Visual-Cortex. Experimental Brain Research. 1972; 15:439-+. [PubMed: 5079475]

Bolz J, Gilbert CD. Generation of End-Inhibition in the Visual-Cortex Via Interlaminar Connections. Nature. 1986; 320:362–365. [PubMed: 3960119]

Borg-Graham LJ, Monier C, Fregnac Y. Visual input evokes transient and strong shunting inhibition in visual cortical neurons. Nature. 1998; 393:369–373. [PubMed: 9620800]

Brainard DH. The psychophysics toolbox. Spatial Vision. 1997; 10:433–436. [PubMed: 9176952]

Bringuier V, Chavane F, Glaeser L, Fregnac Y. Horizontal propagation of visual activity in the synaptic integration field of area 17 neurons. Science. 1999; 283:695–699. [PubMed: 9924031]

Busse L, Ayaz A, Dhruv NT, Katzner S, Saleem AB, Scholvinck ML, Zaharia AD, Carandini M. The Detection of Visual Contrast in the Behaving Mouse. Journal of Neuroscience. 2011; 31:11351–11361. [PubMed: 21813694]

Carandini M, Heeger DJ, Movshon JA. Linearity and normalization in simple cells of the macaque primary visual cortex. The Journal of neuroscience : the official journal of the Society for Neuroscience. 1997; 17:8621–8644. [PubMed: 9334433]

Chadderton P, Schaefer AT, Williams SR, Margrie TW. Sensory-evoked synaptic integration in cerebellar and cerebral cortical neurons. Nature Reviews Neuroscience. 2014; 15:71–83. [PubMed: 24434910]

Chance FS, Abbott LF, Reyes AD. Gain modulation from background synaptic input. Neuron. 2002; 35:773–782. [PubMed: 12194875]

Contreras D, Palmer L. Response to contrast of electrophysiologically defined cell classes in primary visual cortex. The Journal of neuroscience : the official journal of the Society for Neuroscience. 2003; 23:6936–6945. [PubMed: 12890788]

de Kock CPJ, Sakmann B. Spiking in primary somatosensory cortex during natural whisking in awake head-restrained rats is cell-type specific. P Natl Acad Sci USA. 2009; 106:16446–16450.

Douglas RJ, Martin KA, Whitteridge D. An intracellular analysis of the visual responses of neurones in cat visual cortex. The Journal of physiology. 1991; 440:659–696. [PubMed: 1804981]

Durand S, Iyer R, Mizuseki K, de Vries S, Mihalas S, Reid RC. A Comparison of Visual Response Properties in the Lateral Geniculate Nucleus and Primary Visual Cortex of Awake and

Author Manuscript Author Manuscript Author Manuscript Author Manuscript

Anesthetized Mice. The Journal of neuroscience : the official journal of the Society for Neuroscience. 2016; 36:12144–12156. [PubMed: 27903724]

Ferezou I, Bolea S, Petersen CCH. Visualizing the cortical representation of whisker touch: Voltage-sensitive dye imaging in freely moving mice. Neuron. 2006; 50:617–629. [PubMed: 16701211]

Ferster D. Orientation Selectivity of Synaptic Potentials in Neurons of Cat Primary Visual-Cortex. Journal of Neuroscience. 1986; 6:1284–1301. [PubMed: 3711980]

Ferster D, Jagadeesh B. EPSP-IPSP interactions in cat visual cortex studied with in vivo whole-cell patch recording. The Journal of neuroscience : the official journal of the Society for Neuroscience. 1992; 12:1262–1274. [PubMed: 1556595]

Fu Y, Tucciarone JM, Espinosa JS, Sheng NY, Darcy DP, Nicoll RA, Huang ZJ, Stryker MP. A Cortical Circuit for Gain Control by Behavioral State. Cell. 2014; 156:1139–1152. [PubMed: 24630718]

Gilbert CD. Laminar differences in receptive field properties of cells in cat primary visual cortex. The Journal of physiology. 1977; 268:391–421. [PubMed: 874916]

Gradinaru V, Zhang F, Ramakrishnan C, Mattis J, Prakash R, Diester I, Goshen I, Thompson KR, Deisseroth K. Molecular and cellular approaches for diversifying and extending optogenetics. Cell. 2010; 141:154–165. [PubMed: 20303157]

Greenberg DS, Wallace DJ, Kerr JN. Imaging neuronal population activity in awake and anesthetized rodents. Cold Spring Harbor protocols. 2014; 2014:912–922. [PubMed: 25183826]

Haider B, Duque A, Hasenstaub AR, McCormick DA. Neocortical network activity in vivo is generated through a dynamic balance of excitation and inhibition. Journal of Neuroscience. 2006; 26:4535–4545. [PubMed: 16641233]

Haider B, Hausser M, Carandini M. Inhibition dominates sensory responses in the awake cortex. Nature. 2013; 493:97-+. [PubMed: 23172139]

Haider B, Krause MR, Duque A, Yu Y, Touryan J, Mazer JA, McCormick DA. Synaptic and network mechanisms of sparse and reliable visual cortical activity during nonclassical receptive field stimulation. Neuron. 2010; 65:107–121. [PubMed: 20152117]

Hausser M, Roth A. Estimating the time course of the excitatory synaptic conductance in neocortical pyramidal cells using a novel voltage jump method. Journal of Neuroscience. 1997; 17:7606–7625. [PubMed: 9315883]

Higley MJ, Contreras D. Balanced excitation and inhibition determine spike timing during frequency adaptation. Journal of Neuroscience. 2006; 26:448–457. [PubMed: 16407542]

Hirsch JA, Alonso JM, Reid RC, Martinez LM. Synaptic integration in striate cortical simple cells. The Journal of neuroscience : the official journal of the Society for Neuroscience. 1998; 18:9517–9528. [PubMed: 9801388]

Hu H, Cavendish JZ, Agmon A. Not all that glitters is gold: off-target recombination in the somatostatin-IRES-Cre mouse line labels a subset of fast-spiking interneurons. Frontiers in neural circuits. 2013; 7:195. [PubMed: 24339803]

Hubel DH, Wiesel TN. Receptive Fields and Functional Architecture in Two Nonstriate Visual Areas (18 and 19) of the Cat. Journal of neurophysiology. 1965; 28:229–289. [PubMed: 14283058]

Kato HK, Asinof SK, Isaacson JS. Network-Level Control of Frequency Tuning in Auditory Cortex. Neuron. 2017; 95:412–423. e414. [PubMed: 28689982]

Li YT, Liu BH, Chou XL, Zhang LI, Tao HZW. Synaptic Basis for Differential Orientation Selectivity between Complex and Simple Cells in Mouse Visual Cortex. Journal of Neuroscience. 2015; 35:11081–11093. [PubMed: 26245969]

Li YT, Ma WP, Li LY, Ibrahim LA, Wang SZ, Tao HW. Broadening of Inhibitory Tuning Underlies Contrast-Dependent Sharpening of Orientation Selectivity in Mouse Visual Cortex. Journal of Neuroscience. 2012a; 32:16466–16477. [PubMed: 23152629]

Li YT, Ma WP, Pan CJ, Zhang LI, Tao HZW. Broadening of Cortical Inhibition Mediates Developmental Sharpening of Orientation Selectivity. Journal of Neuroscience. 2012b; 32:3981–3991. [PubMed: 22442065]

Litwin-Kumar A, Rosenbaum R, Doiron B. Inhibitory stabilization and visual coding in cortical circuits with multiple interneuron subtypes. Journal of neurophysiology. 2016; 115:1399–1409. [PubMed: 26740531]

Author Manuscript Author Manuscript Author Manuscript Author Manuscript

Liu BH, Li PY, Li YT, Sun YJJ, Yanagawa Y, Obata K, Zhang LI, Tao HZW. Visual Receptive Field Structure of Cortical Inhibitory Neurons Revealed by Two-Photon Imaging Guided Recording. Journal of Neuroscience. 2009; 29:10520–10532. [PubMed: 19710305]

Liu BH, Li PY, Sun YJJ, Li YT, Zhang LI, Tao HW. Intervening inhibition underlies simple-cell receptive field structure in visual cortex. Nature Neuroscience. 2010; 13:89–U256. [PubMed: 19946318]

Maffei L, Fiorentini A. The visual cortex as a spatial frequency analyser. Vision research. 1973; 13:1255–1267. [PubMed: 4722797]

Maffei L, Fiorentini A. The unresponsive regions of visual cortical receptive fields. Vision research. 1976; 16:1131–1139. [PubMed: 969225]

Margrie TW, Brecht M, Sakmann B. In vivo, low-resistance, whole-cell recordings from neurons in the anaesthetized and awake mammalian brain. Pflug Arch Eur J Phy. 2002; 444:491–498.

Marino J, Schummers J, Lyon DC, Schwabe L, Beck O, Wiesing P, Obermayer K, Sur M. Invariant computations in local cortical networks with balanced excitation and inhibition. Nature Neuroscience. 2005; 8:194–201. [PubMed: 15665876]

Niell CM, Stryker MP. Highly selective receptive fields in mouse visual cortex. The Journal of neuroscience : the official journal of the Society for Neuroscience. 2008; 28:7520–7536. [PubMed: 18650330]

Niell CM, Stryker MP. Modulation of visual responses by behavioral state in mouse visual cortex. Neuron. 2010; 65:472–479. [PubMed: 20188652]

Nienborg H, Hasenstaub A, Nauhaus I, Taniguchi H, Huang ZJ, Callaway EM. Contrast Dependence and Differential Contributions from Somatostatin- and Parvalbumin-Expressing Neurons to Spatial Integration in Mouse V1. Journal of Neuroscience. 2013; 33:11145–11154. [PubMed: 23825418]

Nurminen L, Angelucci A. Multiple components of surround modulation in primary visual cortex: Multiple neural circuits with multiple functions? Vision research. 2014; 104:47–56. [PubMed: 25204770]

Okun M, Lampl I. Instantaneous correlation of excitation and inhibition during ongoing and sensory-evoked activities. Nature Neuroscience. 2008; 11:535–537. [PubMed: 18376400]

Ozeki H, Finn IM, Schaffer ES, Miller KD, Ferster D. Inhibitory stabilization of the cortical network underlies visual surround suppression. Neuron. 2009; 62:578–592. [PubMed: 19477158]

Ozeki H, Sadakane O, Akasaki T, Naito T, Shimegi S, Sato H. Relationship between excitation and inhibition underlying size tuning and contextual response modulation in the cat primary visual cortex. The Journal of neuroscience : the official journal of the Society for Neuroscience. 2004; 24:1428–1438. [PubMed: 14960615]

Paken JMP, Lowe SC, Dylda E, Keemink SW, Currie SP, Coutts CA, Rochefort NL. Behavioral-state modulation of inhibition is context-dependent and cell type specific in mouse visual cortex. Elife. 2016; 5

Perrenoud Q, Pennartz CMA, Gentet LJ. Membrane Potential Dynamics of Spontaneous and Visually Evoked Gamma Activity in V1 of Awake Mice. Plos Biol. 2016; 14

Petreanu L, Mao T, Sternson SM, Svoboda K. The subcellular organization of neocortical excitatory connections. Nature. 2009; 457:1142–1145. [PubMed: 19151697]

Pfeffer CK, Xue MS, He M, Huang ZJ, Scanziani M. Inhibition of inhibition in visual cortex: the logic of connections between molecularly distinct interneurons. Nature neuroscience. 2013; 16:1068–U1130. [PubMed: 23817549]

Polack PO, Friedman J, Golshani P. Cellular mechanisms of brain state-dependent gain modulation in visual cortex. Nature Neuroscience. 2013; 16:1331–U1227. [PubMed: 23872595]

Poleg-Polsky A, Diamond JS. Imperfect Space Clamp Permits Electrotonic Interactions between Inhibitory and Excitatory Synaptic Conductances, Distorting Voltage Clamp Recordings. PloS one. 2011; 6

Priebe NJ, Ferster D. Direction selectivity of excitation and inhibition in simple cells of the cat primary visual cortex. Neuron. 2005; 45:133–145. [PubMed: 15629708]

Reimer J, Froudarakis E, Cadwell CR, Yatsenko D, Denfield GH, Tolias AS. Pupil Fluctuations Track Fast Switching of Cortical States during Quiet Wakefulness. Neuron. 2014; 84:355–362. [PubMed: 25374359]

Author Manuscript Author Manuscript Author Manuscript Author Manuscript

Rubin DB, Van Hooser SD, Miller KD. The Stabilized Supralinear Network: A Unifying Circuit Motif Underlying Multi-Input Integration in Sensory Cortex. Neuron. 2015; 85:402–417. [PubMed: 25611511]

Sato TK, Haider B, Hausser M, Carandini M. An excitatory basis for divisive normalization in visual cortex. Nature Neuroscience. 2016; 19:568-+. [PubMed: 26878671]

Sceniak MP, Ringach DL, Hawken MJ, Shapley R. Contrast's effect on spatial summation by macaque V1 neurons. Nature neuroscience. 1999; 2:733–739. [PubMed: 10412063]

Sekerli M, Del Negro CA, Lee RH, Butera RJ. Estimating action potential thresholds from neuronal time-series: New metrics and evaluation of methodologies. Ieee T Bio-Med Eng. 2004; 51:1665–1672.

Shu YS, Hasenstaub A, McCormick DA. Turning on and off recurrent balanced cortical activity. Nature. 2003; 423:288–293. [PubMed: 12748642]

Shushruth S, Mangapathy P, Ichida JM, Bressloff PC, Schwabe L, Angelucci A. Strong Recurrent Networks Compute the Orientation Tuning of Surround Modulation in the Primate Primary Visual Cortex. Journal of Neuroscience. 2012; 32:308–321. [PubMed: 22219292]

Smith SL, Smith IT, Branco T, Hausser M. Dendritic spikes enhance stimulus selectivity in cortical neurons in vivo. Nature. 2013; 503:115-+. [PubMed: 24162850]

Sun YJ, Wu GK, Liu BH, Li P, Zhou M, Xiao Z, Tao HW, Zhang LI. Fine-tuning of pre-balanced excitation and inhibition during auditory cortical development. Nature. 2010; 465:927–U928. [PubMed: 20559386]

Tsodyks MV, Skaggs WE, Sejnowski TJ, McNaughton BL. Paradoxical effects of external modulation of inhibitory interneurons. The Journal of neuroscience : the official journal of the Society for Neuroscience. 1997; 17:4382–4388. [PubMed: 9151754]

Vaiceliunaite A, Erisken S, Franzen F, Katzner S, Busse L. Spatial integration in mouse primary visual cortex. Journal of neurophysiology. 2013; 110:964–972. [PubMed: 23719206]

Veit J, Hakim R, Jadi MP, Sejnowski TJ, Adesnik H. Cortical gamma band synchronization through somatostatin interneurons. Nature neuroscience. 2017

Vinck M, Batista-Brito R, Knoblich U, Cardin JA. Arousal and Locomotion Make Distinct Contributions to Cortical Activity Patterns and Visual Encoding. Neuron. 2015; 86:740–754. [PubMed: 25892300]

Wehr M, Zador AM. Balanced inhibition underlies tuning and sharpens spike timing in auditory cortex. Nature. 2003; 426:442–446. [PubMed: 14647382]

Williams SR, Mitchell SJ. Direct measurement of somatic voltage clamp errors in central neurons. Nature neuroscience. 2008; 11:790–798. [PubMed: 18552844]

Wu GK, Arbuckle R, Liu BH, Tao HW, Zhang LI. Lateral sharpening of cortical frequency tuning by approximately balanced inhibition. Neuron. 2008; 58:132–143. [PubMed: 18400169]

Author Manuscript Author Manuscript Author Manuscript Author Manuscript

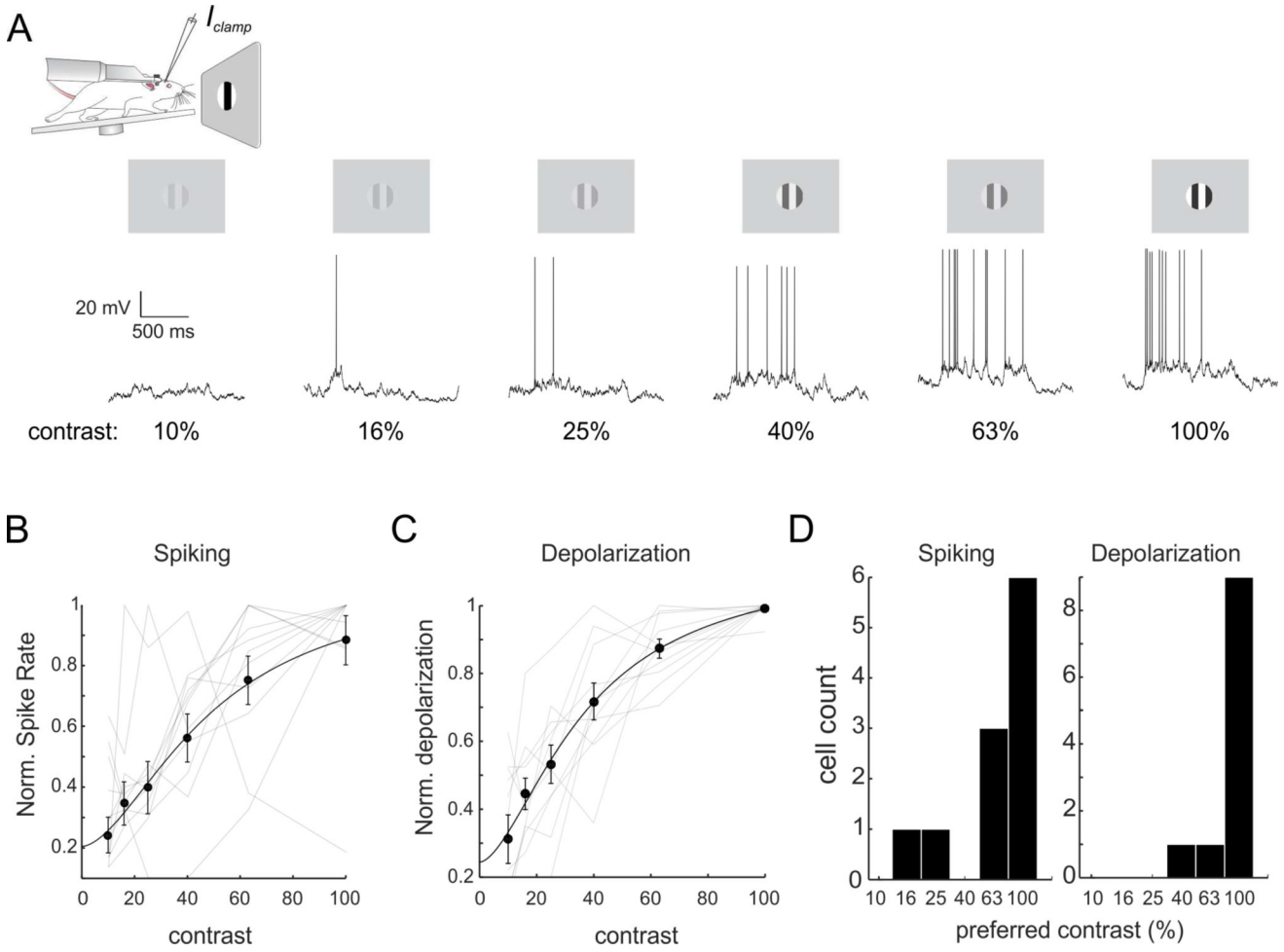

Figure 1. The membrane potential and spiking of L2/3 visual cortical neurons monotonically increase with higher contrasts

A) Top: schematic of the recording configuration in awake, head-fixed mice free to run on a circular treadmill. Middle: representations of the six visual stimuli of fixed size and orientation, but varying contrast. Bottom: Example traces of the membrane potential and spiking activity of one neuron to the six contrast levels. B) Plot of the mean spike rate versus contrast (n = 11 cells). Gray traces are tuning curves from individual cells. C) As in B) but for mean membrane potential during the stimulus. D) Left: Histogram of the preferred contrast for the spiking activity of the 11 recorded cells. Right: As at left, but for the mean depolarization of the membrane potential. Error bars are s.e.m.

Author Manuscript Author Manuscript Author Manuscript Author Manuscript

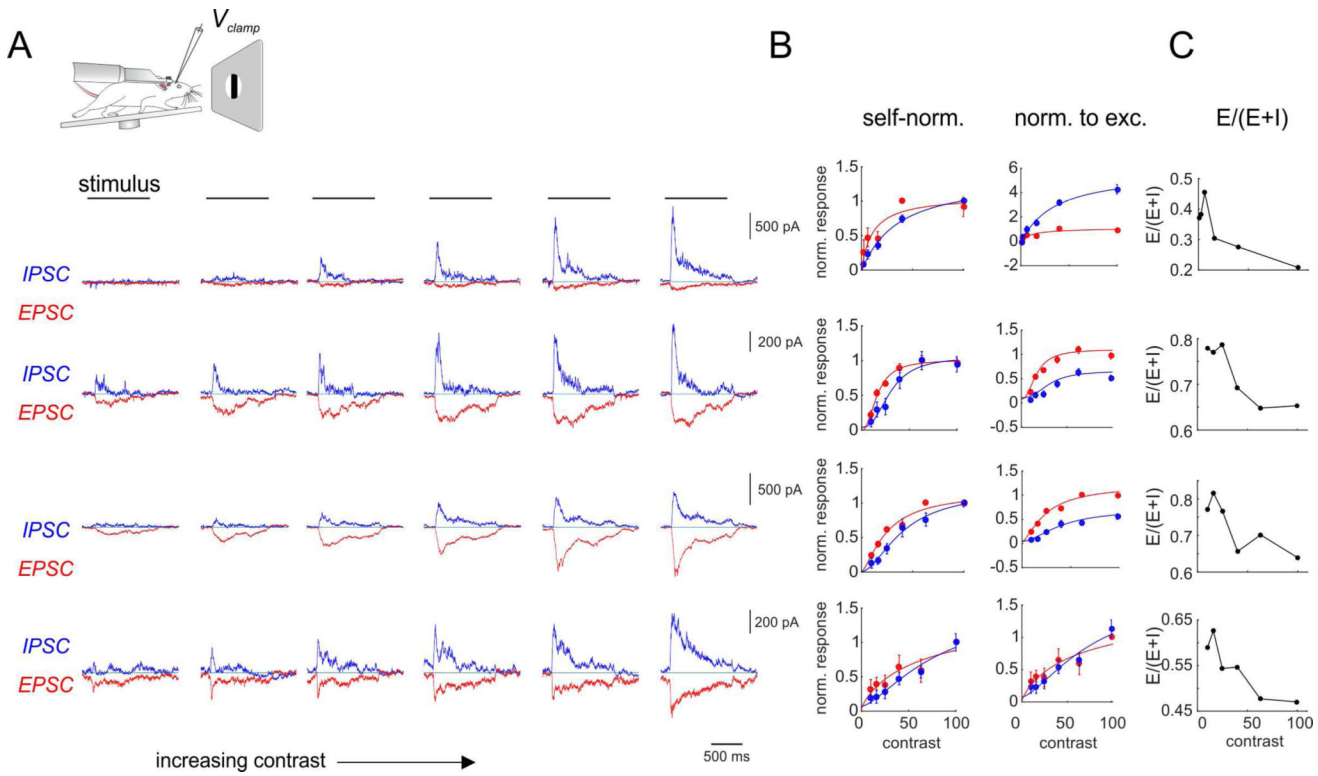

Figure 2. Examples of synaptic responses with increasing stimulus contrast

A) Top: recording schematic. Bottom: Four sets of example traces from four different cells showing synaptic excitation (red) or inhibition (blue) for six levels of increasing contrast. The black line indicates the visual stimulus period and the analysis period. The light blue line indicates the zero point. B) Plots of the mean *E* and *I* across contrast for the cells whose average traces are shown in A). Left: *E* and *I* normalized to their own peak values. Right: *E* and *I* normalized to the peak of *E*. The analysis period is the first second after the onset of the visual stimulus. C) Plots of the E/I ratio versus stimulus contrast for the four example cells. Error bars are s.e.m.

Author Manuscript Author Manuscript Author Manuscript Author Manuscript

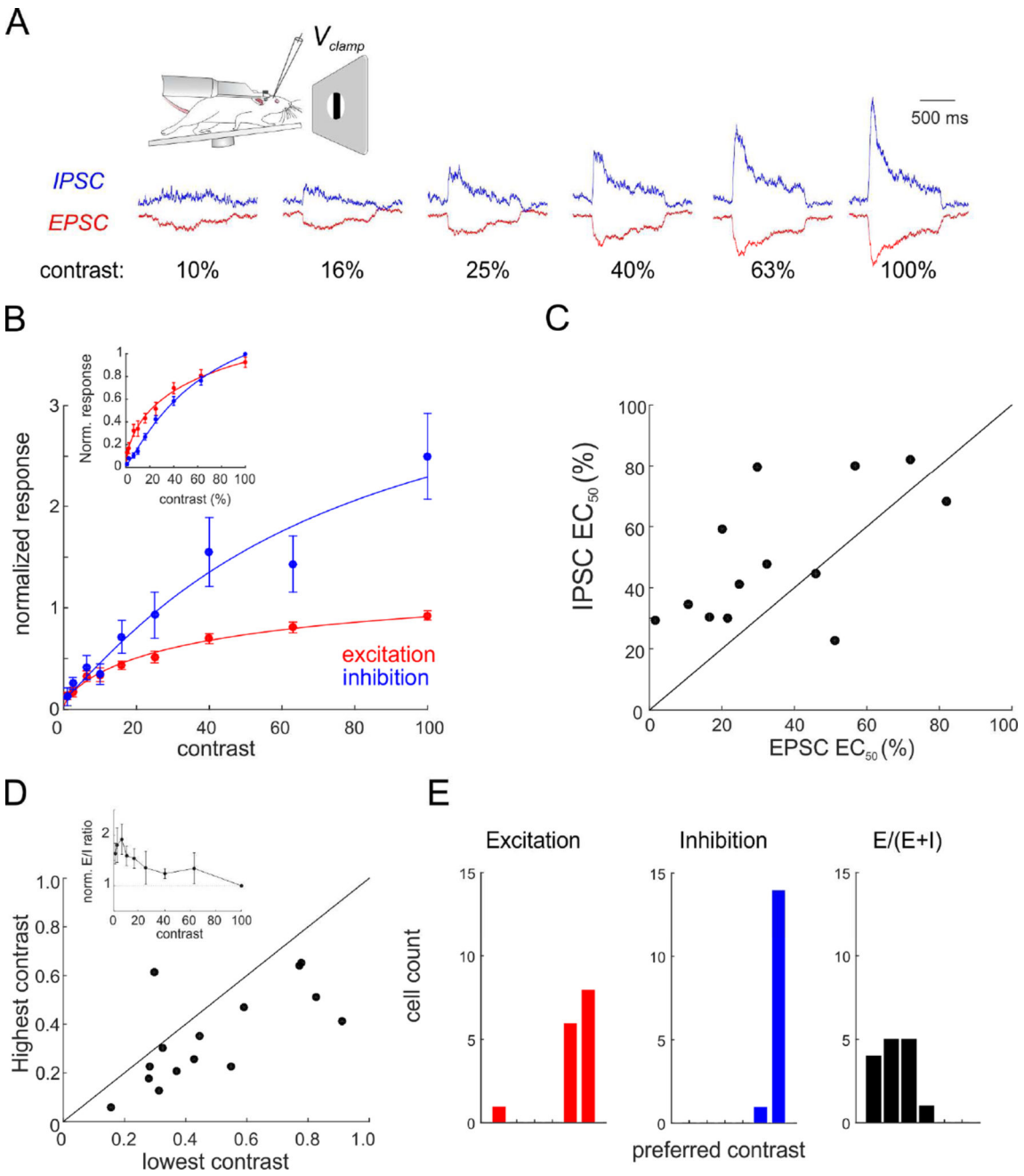

Figure 3. Excitation and inhibition monotonically increase with stimulus contrast, while the E/I ratio decreases

A) Top: experimental schematic. Bottom: Grand average normalized traces of synaptic excitation (red) or inhibition (blue) computed across all recorded cells (n = 12) for six levels of contrast. B) Plot of average excitation (red) and inhibition (blue), across the 15 recorded cells, normalized to the max of excitation in each cell. Inset: *E* and *I* normalized to their own peak values. C) Scatter plot of the estimated EC_{50} of synaptic excitation and inhibition across 13/15 of the recorded cells with good fits ($p < 0.05$, Wilcoxon sign rank test). D) Plot of the E/I ratio for all 15 cells. Inset: Normalized E/I ratio as a function of contrast. E)

Histogram of the preferred contrast for synaptic excitation (left), inhibition (middle), and the E/I ratio (right). Error bars are s.e.m.

Author Manuscript Author Manuscript Author Manuscript Author Manuscript

Author Manuscript Author Manuscript Author Manuscript Author Manuscript

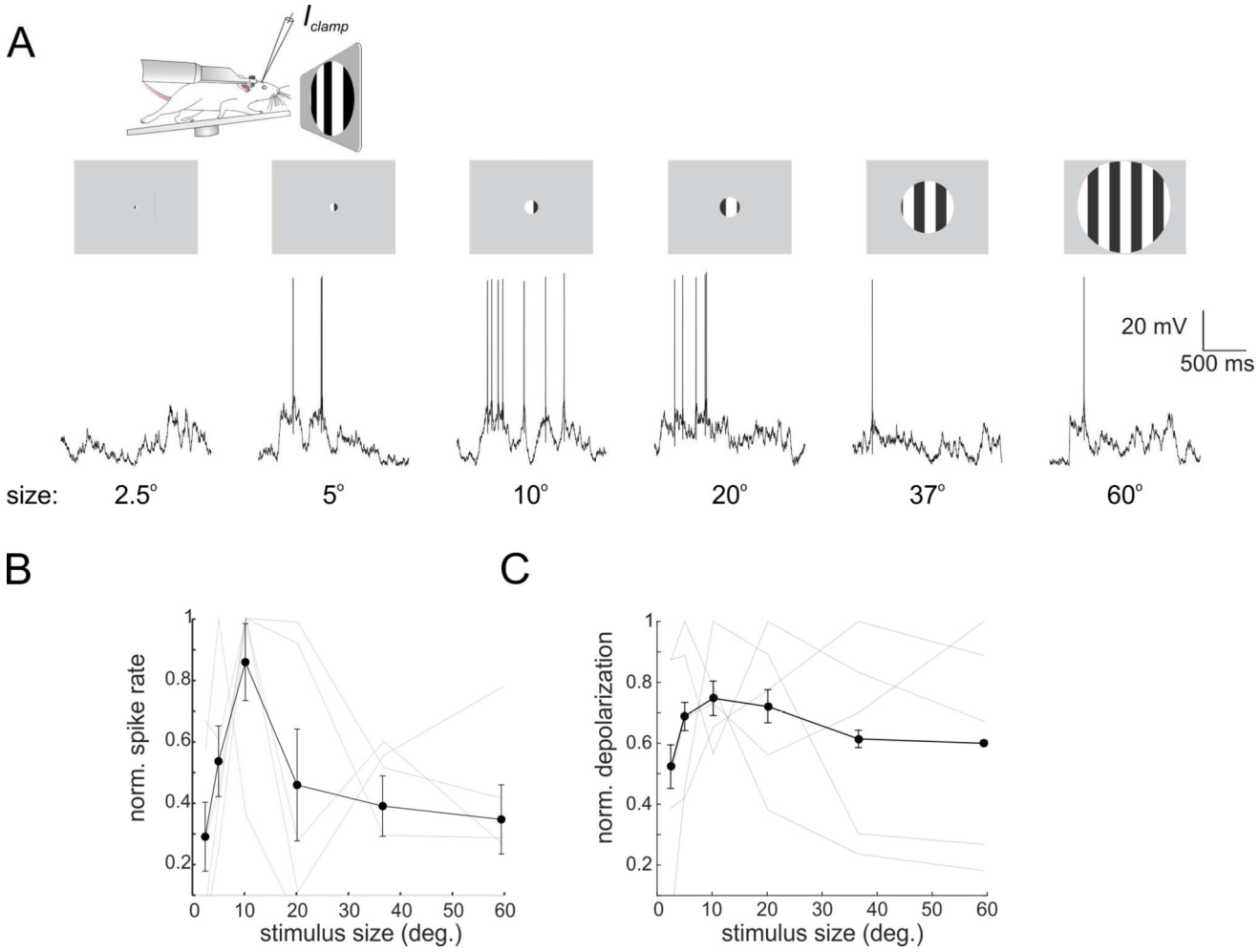

Figure 4. The membrane potential and spiking of L2/3 visual cortical neurons are tuned to smaller sizes

A) Top: experimental schematic. Middle: representations of the six drifting visual stimuli of fixed contrast and orientation, but varying size. Bottom: Example traces of the membrane potential and spiking activity of one neuron to the six stimulus sizes. B) Plot of the mean spike rate vs. size (n = 5 cells). Gray traces are tuning curves from individual cells. C) As in B) but for the mean membrane potential during the stimulus. Error bars are s.e.m.

Author Manuscript Author Manuscript Author Manuscript Author Manuscript

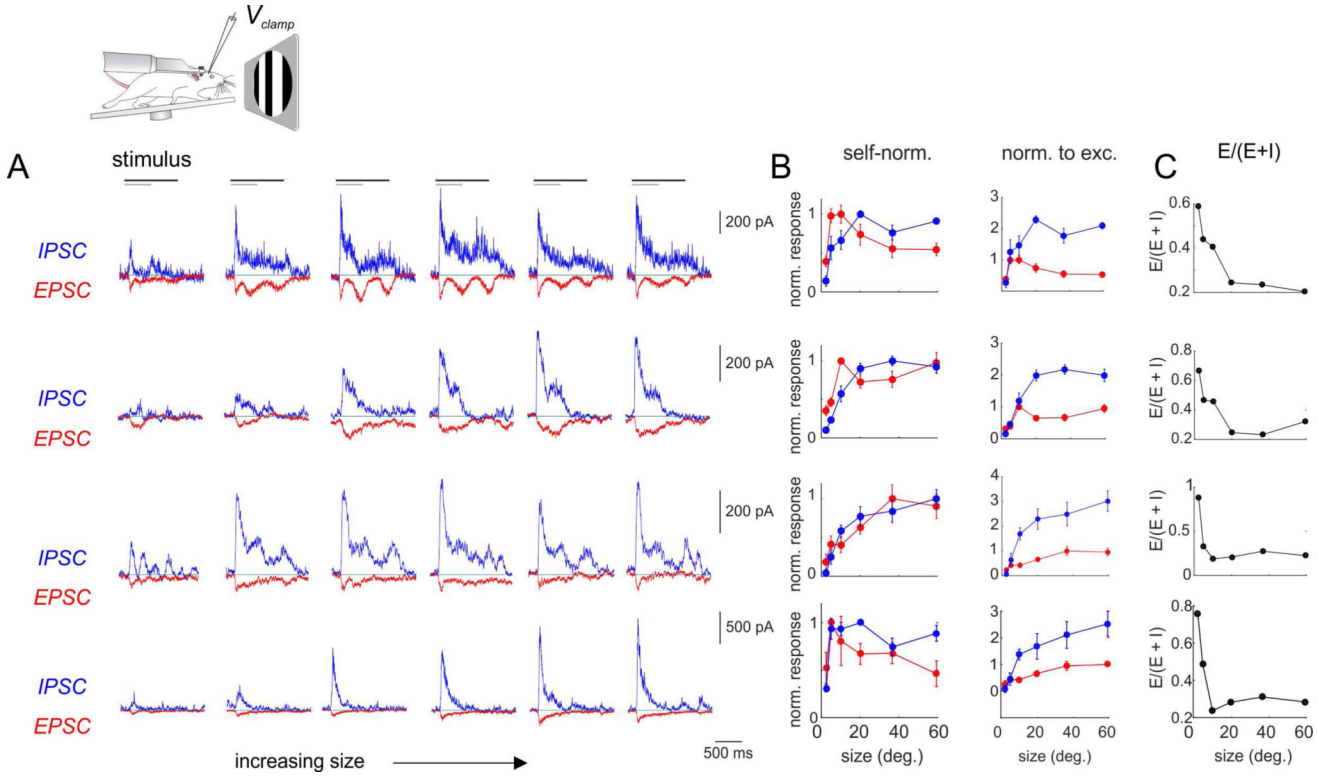

Figure 5. Examples of synaptic responses with increasing stimulus size

A) Top: recording schematic. Bottom: Four sets of example traces from four different cells showing synaptic excitation (red) or inhibition (blue) for six stimulus sizes. The black bar indicates the visual stimulus, and the grey bar indicates the period of analysis. B) Plots of the mean *E* and *I* across sizes for the cells whose average traces are shown in A). Left: *E* and *I* normalized to their own peak values. Right: *E* and *I* normalized to the peak of E. C) Plots of the E/I ratio versus stimulus size for each example cell. Error bars are s.e.m.

Author Manuscript Author Manuscript Author Manuscript Author Manuscript

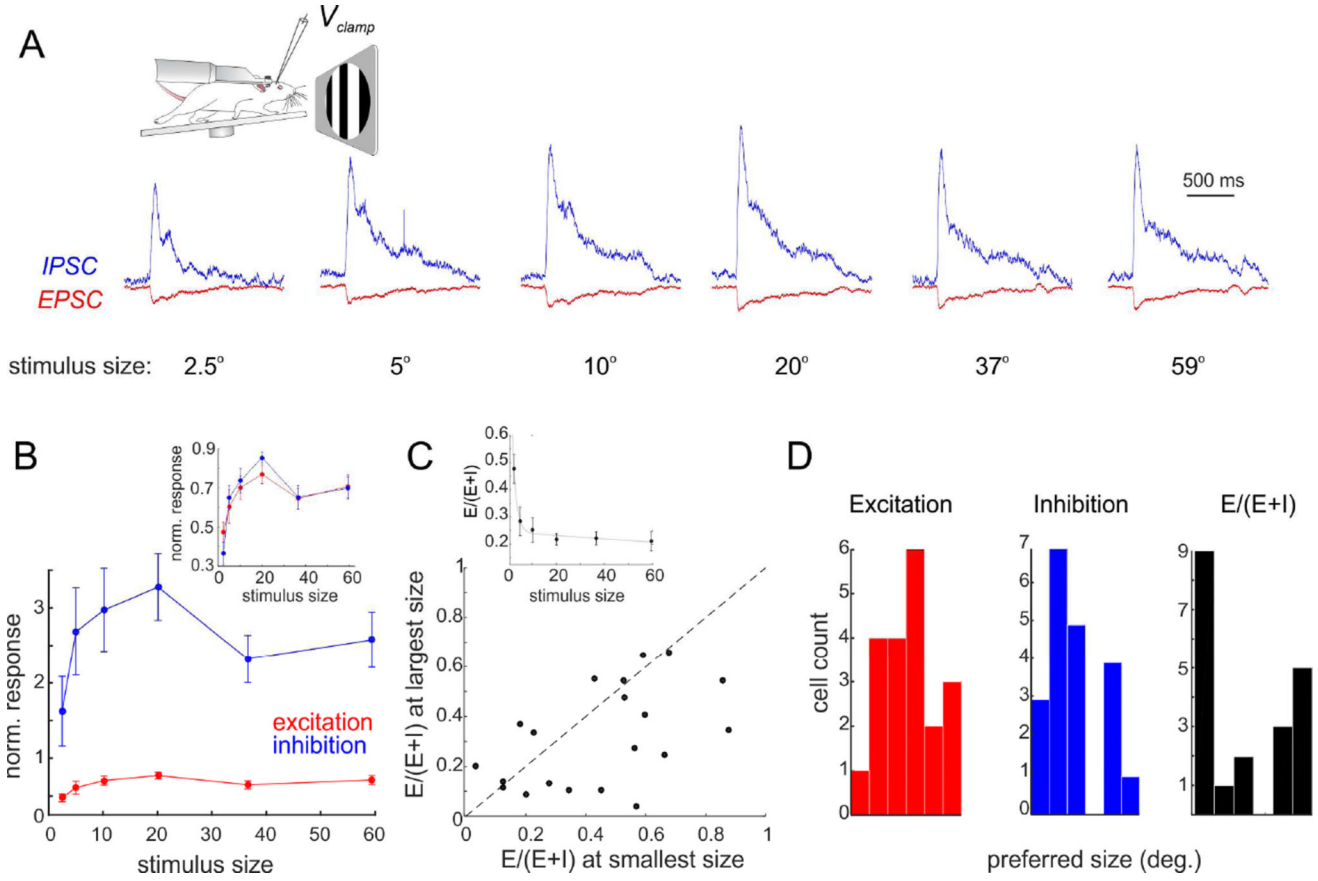

Figure 6. The E/I ratio declines with increasing stimulus size

A) Top: experimental schematic. Bottom: Grand average normalized traces of synaptic excitation (red) or inhibition (blue) computed across all recorded cells (n = 20) for six stimulus sizes. B) Plot of average excitation (red) and inhibition (blue), across the 20 recorded cells, normalized to maximal excitation in each cell. Inset: *E* and *I* normalized to their peak values. C) Plot of the E/I ratio across the same 20 cells. Inset: E/I ratio as a function of size for all cells exhibiting their maximum ratio at the smallest size (n = 9 cells). D) Histogram of the preferred size for synaptic excitation (left), inhibition (middle), and corresponding E/I ratio (right).

Author Manuscript Author Manuscript Author Manuscript Author Manuscript

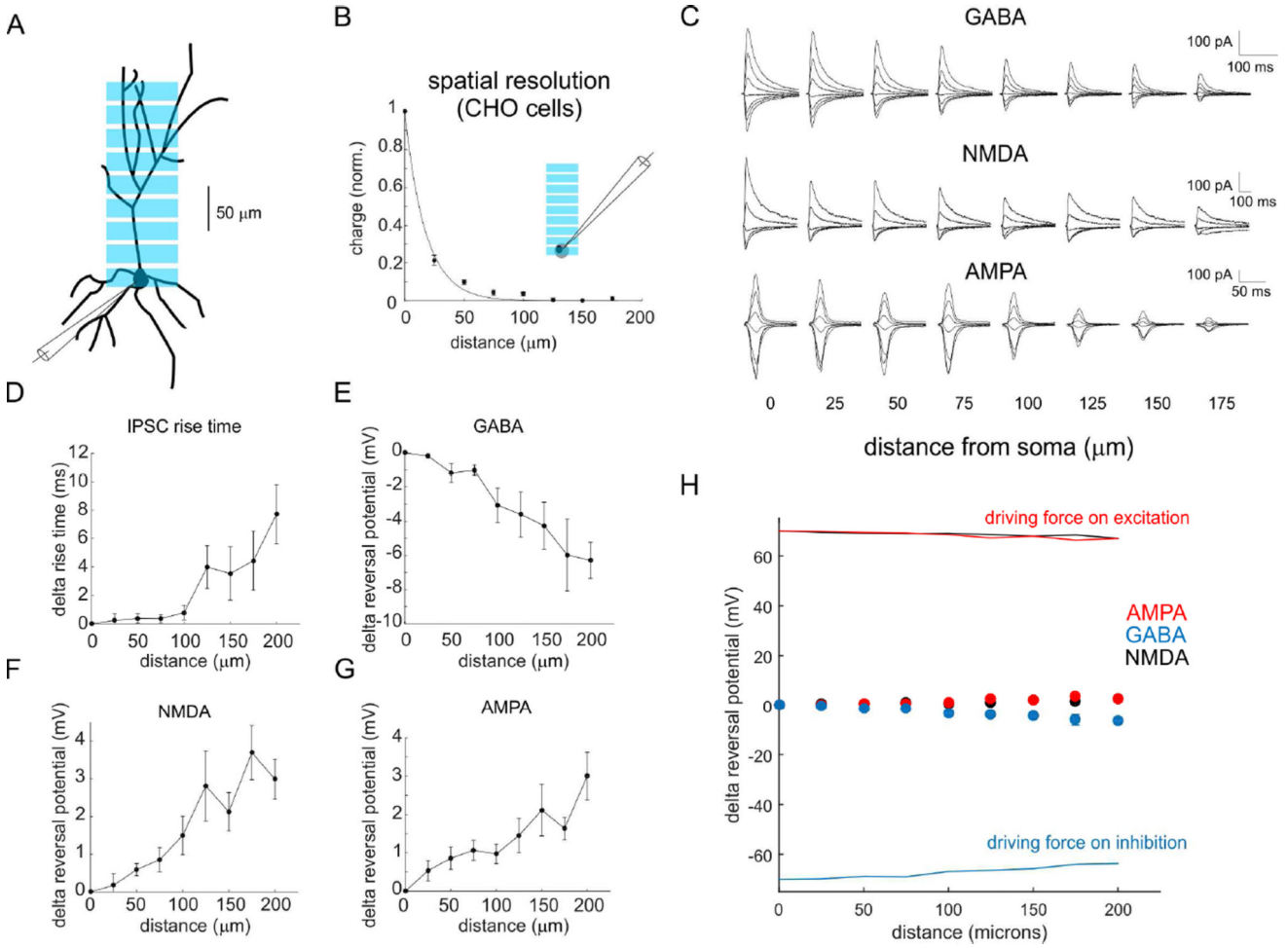

Figure 7. The somatic voltage clamp adequately separates excitation from inhibition in L2/3 pyramidal neurons

A) Experiment schematic. A L2/3 pyramidal neuron is patched with a somatic voltage clamp electrode, while excitatory or inhibitory synapses at defined distances from the soma are photo-stimulated with the sCRACM approach using a rectangular light bar projected via a digital-micromirror device. B) Measurement of the spatial resolution of the photo-stimulation system: plot of the light-induced charge in ChR2-expressing CHO cells (n = 7) when projecting the optical stimulus at defined distances from the cell. C) Example families of light-induced synaptic currents for GABA, NMDA, and AMPA currents. Each family represents traces taken at a series of command voltages at different distances from the soma. D) Plot of the estimated change in rise time of the IPSC as a function of distance from the soma (n = 6, $p < 0.05$, Kruskal-Wallis). E–F) Plot of the difference of the measured reversal potential for the specified current as compared to the measured value when the light stimulus was on the soma and proximal dendrites (GABA: n = 6; NMDA: n = 6; AMPA: n = 7; $p < 0.05$ for each, Kruskal-Wallis). H) The plots from E–G are re-plotted on one axis relative to the estimated effective driving force when measuring excitation and inhibition by clamping at either −70 mV or 0 mV, respectively.

Author Manuscript Author Manuscript Author Manuscript Author Manuscript

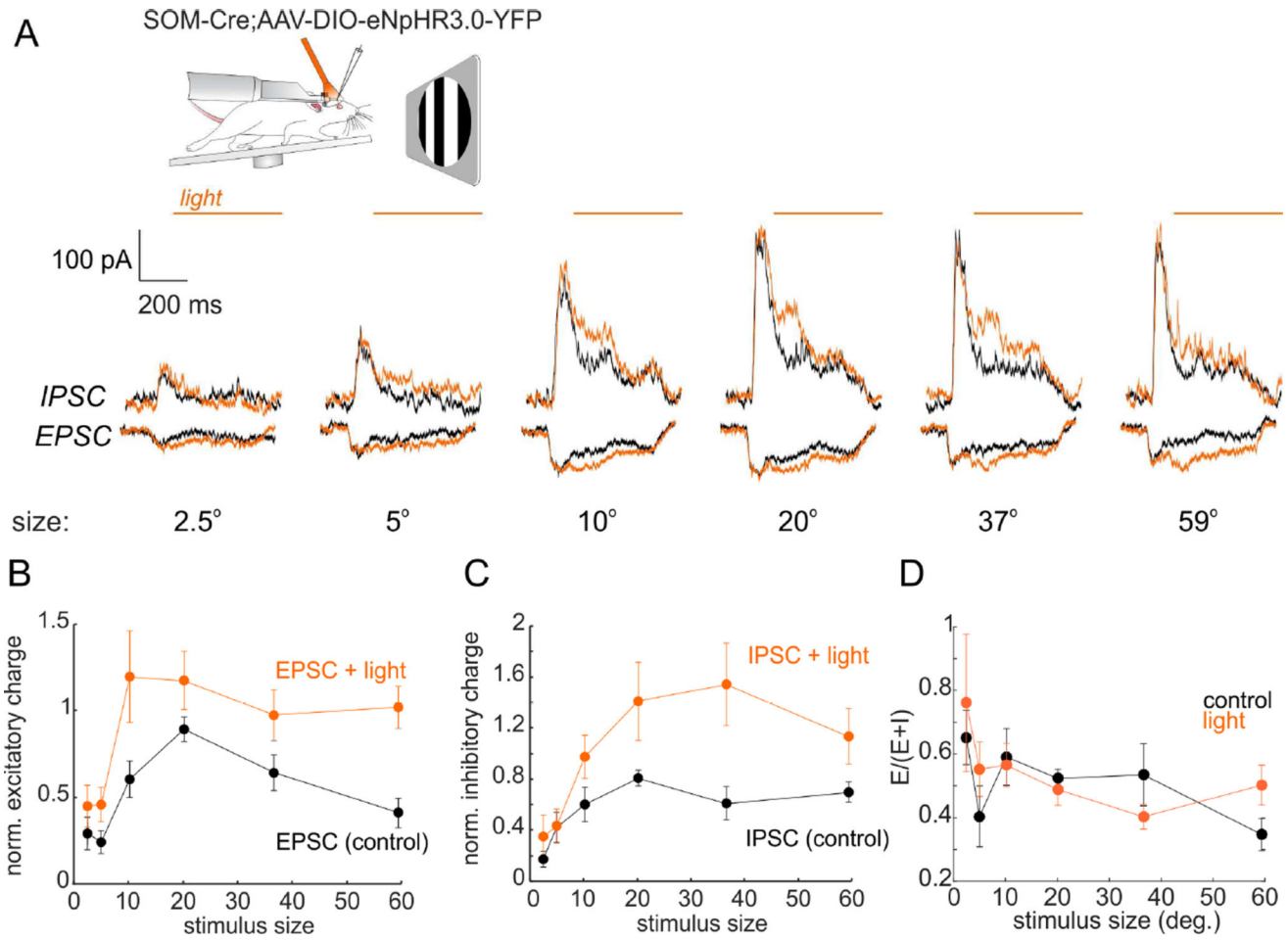

Figure 8.

Optogenetic suppression of SOM interneurons enhances synaptic excitation and inhibition. A) Top: recording schematic. Bottom: grand average traces of excitation and inhibition in control conditions (black) and during photo-suppression of SOM cells (orange) for six stimulus sizes. B) Plot of the average excitation across the six sizes under control conditions (black) and during SOM cell suppression (orange), n = 7 cells. C) as in B) but for synaptic inhibition ($p < 0.05$). D) E/I ratio under control (black) and light (orange) conditions, ($p = 0.5$, n = 7). Error bars are s.e.m.